High-Performance GOCE Gravity Field Recovery from Gravity Gradient Tensor Invariants and Kinematic Orbit Information

Oliver Baur and Erik W. Grafarend

Stuttgart University, Geodetic Department, Geschwister-Scholl-Str.24D,
70174 Stuttgart, baur@gis.uni-stuttgart.de

Summary. The GOCE mission, planned to be launched in autumn 2006, will allow to determine the static Earth gravity field down to features of 100 km–70 km (half wavelength) in terms of spatial resolution. Since satellite gradiometry is restricted to the medium- to short-wavelength part of the gravitational spectrum, only its combination with satellite-to-satellite measurements in the high-low mode will meet the mission requirements as demanded by the ESA, namely a high-accurate GOCE-only terrestrial gravity field modeling. Here we apply the acceleration approach which is predominantly characterized by numerical differentiation of the kinematic GOCE orbit. Gradiometry is treated by analysis of the fundamental invariants of the gravitational tensor. These quantities neither depend on reference frame rotations nor on the orientation of the gradiometer frame in space. Linearization, computational effort and amalgamation of tensor elements provided with different levels of accuracy make this approach hard to handle. The use of high performance computing facilities, parallel programming standards and optimized numerical libraries are the key to accomplish efficient gravity field recovery.

Key words: GOCE-only Solution, Tensor Invariants, Kinematic Orbit Analysis, Numerical Differentiation, High Performance Computing

1 Introduction

Within ESA's (European Space Agency) "Living Planet" program the Earth explorer core mission GOCE (Gravity field and steady-state Ocean Circulation Explorer) planned to be launched in autumn 2006 will be the first satellite mission applying three-dimensional gradiometry in space (ESA, 1999, 2000). The observation data collected by the on-board sensors during the operational mode covering two six-month periods, interrupted by a hibernation phase of the satellite, is expected to allow for the recovery of the static terrestrial gravity field down to features of 100 km–70 km in terms of spatial resolution (half wavelength). However, satellite gravity gradiometry (SGG) is not able to recover the long-wavelength part of the Earth gravity field due to the limited

measurement band width (MBW) of the gradiometer instrument ranging from 5 mHz to 0.1 Hz. Thus, a GOCE-only gravity field solution as demanded as the mission outcome by the ESA can't be provided by gradiometry alone.

Actually, the CHAMP (CHAllenging Minisatellite Payload) satellite mission established the opportunity to develop adequate algorithms for satellite-to-satellite tracking analysis in the high-low mode (hl-SST) between the high orbiting Global Positioning System (GPS) satellites and the low Earth orbiter (LEO) CHAMP (Reigber et al., 2005). Different approaches showed comparable results for the modeling of the long-wavelength part of the terrestrial gravity field such as the energy balance method (Földvary et al., 2005), short-arc analysis (Mayer-Gürr et al., 2005) and the acceleration approach (Reubelt et al., 2005). Within the scope of this contribution we focus on the acceleration approach. It is predominantly characterized by 2^{nd} order numerical differentiation of the kinematic satellite orbit. The GPS track of the GOCE spacecraft is used to complement gradiometer observations in the dedicated frequency domain. The combined analysis of both SGG and hl-SST measurements is able to provide a GOCE-only estimate of the Earth's gravity field covering the whole gravitational spectrum.

Commonly, SGG analysis is performed on the level of gravitational gradients (GGs), namely the main diagonal elements of the gravitational tensor, being provided with highest accuracy with respect to the gradiometer frame of reference. A completely different approach is based on the rotational invariants of the observation tensor (Rummel et al., 1986). Beyond a pure methodological interest and the challenges of an efficient implementation, the main motivation for this approach is twofold. Firstly, the invariance under rotations actually means that knowledge about the gradiometer frame orientation is not required, neither with respect to the orbit frame nor to inertial space. Secondly, since this method has not been implemented before, it is independent of more conventional time-wise and space-wise approaches.

With the design and realization of the GOCE mission computational tasks gain evident importance in Satellite Geodesy, namely the access to and use of high performance computing (HPC) facilities. Due to the hardware limitations of ordinary personal computers (PCs) concerning both performance and main memory availability, only multiprocessor systems provide high-resolution gravity field estimates within a reasonable time frame.

The paper is organized as follows. The next Section deals with kinematic orbit analysis, predominantly with regard to numerical differentiation techniques to derive satellite accelerations from position information. Section 3 addresses to SGG data analysis based on the rotational invariants of the gravitational tensor. Parallel implementation of the algorithm using HPC facilities is treated in Sect. 4. Finally, the conclusions of this contribution are summarized in Sect. 5.

2 Kinematic Orbit Analysis

This Section is dedicated to the hl-SST part of the GOCE mission. First, the functional model for kinematic orbit analysis is derived followed by studies concerning numerical differentiation techniques. Finally GOCE hl-SST gravity field solutions based on the acceleration approach are presented.

2.1 Methodology

Conventionally, the parameterization of the terrestrial gravitational potential is expressed in spherical coordinates (λ, φ, r) with the unknown potential coefficients u_{lm}, cf. (1). Series truncation at a certain maximal degree $L = l_{\max}$ provides an approximation to reality. Both the geocentric constant GM and the mean Earth radius R are fixed. The normalized Legendre functions of the first kind $\bar{P}_{lm}(\sin\varphi)$ are part of the orthonormal base functions $e_{lm}(\lambda, \varphi)$, dentoted as surface spherical harmonics (2).

$$U_{\mathrm{E}}(\lambda, \varphi, r) = \frac{GM}{R} \sum_{l=0}^{\infty} \sum_{m=-l}^{l} \left(\frac{R}{r}\right)^{l+1} e_{lm}(\lambda, \varphi) u_{lm} \tag{1}$$

$$e_{lm}(\lambda, \varphi) = \begin{cases} \bar{P}_{lm}(\sin\varphi)\cos m\lambda & 0 \le m \le l \\ \bar{P}_{l|m|}(\sin\varphi)\sin|m|\,\lambda & -l \le m < 0 \end{cases} \tag{2}$$

According to (3) the acceleration $\ddot{\mathbf{x}}(t) = \ddot{\mathbf{x}}(\lambda(t), \varphi(t), r(t))$ of the satellite (reduced by all disturbing effects such as tidal forces) is equal to the terrestrial attraction, namely the gradient of the Earth's gravitational potential $U_{\mathrm{E}}(\lambda, \varphi, r)$. Equation (3) is referred to as the acceleration approach and has been proven to perform well for CHAMP gravity field recovery (Reubelt et al., 2005). Kinematic orbit analysis is restricted to the determination of the long-wavelength part of the terrestrial gravity field only due to the satellite's positioning accuracy limited to some centimeters.

$$\begin{aligned} \frac{\mathrm{d}^2}{\mathrm{d}t^2}\left(\mathbf{e}_i x_i(t)\right) &= \mathbf{e}_i \frac{\mathrm{d}^2}{\mathrm{d}t^2} x_i(t) = \mathbf{e}_i \ddot{x}_i(t) = \operatorname{grad} U_{\mathrm{E}}(\lambda, \varphi, r) \\ &= \frac{GM}{R} \sum_{l=0}^{\infty} \sum_{m=-l}^{l} \left(\frac{R}{r}\right)^{l+2} \\ &\times \left\{ \mathbf{e}_\lambda \frac{\partial e_{lm}(\lambda, \varphi)}{\cos\varphi\, \partial\lambda} + \mathbf{e}_\varphi \frac{\partial e_{lm}(\lambda, \varphi)}{\partial\varphi} - \mathbf{e}_r (l+1) e_{lm}(\lambda, \varphi) \right\} u_{lm} \end{aligned} \tag{3}$$

2.2 Numerical Differentiation

The crucial point in (3) is the determination of accelerations $\mathbf{e}_i \ddot{x}_i(t)$ that serve as pseudo-observations for kinematic orbit analysis. Since hl-SST provides orbit information on the level of position coordinates, numerical differentiation techniques have to be applied. GPS positions are highly correlated, predominantly due to systematic atmospheric effects. With regard to

numerical differentiation these errors can be reduced dramatically when using coordinate differences $\Delta\mathbf{x}(t_i) = \mathbf{x}(t_i) - \mathbf{x}(t_{i-1})$ instead of the absolute orbit information (Reubelt et al., 2003). Assuming the remaining systematic errors to be negligible the uncertainties of hl-SST phase measurements itself dominate the overall error budget. These random errors have to be assumed as non-correlated. However, dependent on the procedure for GOCE orbit determination based on GPS phase measurements the positions of the spacecraft will be more or less correlated. Normal distributed position errors, denoted as white noise, can be considered as the worst case. Thus, that scenario is defined as lower bound for what can be expected at least from GOCE hl-SST analysis by means of the acceleration approach. The standard deviation of random position errors is about σ_{x_i} =1-2 cm for each coordinate x_i (ESA, 1999). In most methods for numerical differentiation an interpolative polynomial is fitted through the time-series of position coordinates. A moderate number of sampling points is used to estimate the polynomial coefficients. Due to the oscillation of the polynomial at its edges, the interpolation point is specified to be in the middle of the interpolation mask which is shifted for successive satellite positions. Evaluation of polynomial derivatives finally leads to the desired pseudo-observations.

Besides the number of sampling points, the degree of the polynomial respectively, the methods for numerical differentiation predominantly differ in the kind of the interpolation polynomial, namely its smoothing behavior. Four methods have been explored in detail: (i) Gregory-Newton interpolation, (ii) spline interpolation, (iii) polynomial regression and (iv) smoothing spline interpolation. The non-smoothing methods (i) and (ii) achieve similar results as well as the smoothing methods (iii) and (iv). Thus, in the following solely Gregory-Newton (GN) interpolation (Maeß, 1988) and polynomial regression (PR) will be addressed. Actually, GN is a special case of PR, namely the least squares adjustment to estimate the polynomial coefficients is reduced to a unique estimate. For each coordinate x_i, $i = 1, 2, 3$ Table 1 contains root-mean-square (RMS) values of 500 000 acceleration residuals $\Delta\ddot{\mathbf{x}} = \ddot{\mathbf{x}}^{\text{true}} - \ddot{\mathbf{x}}^{\text{est}}$ between true accelerations $\ddot{\mathbf{x}}^{\text{true}}$ known from orbit simulation and estimated accelerations $\ddot{\mathbf{x}}^{\text{est}}$ applying GN, respectively PR (interpolation interval $\Delta t = 5$ s). Obviously, smoothing methods seem to be by far better suited for numerical differentiation than non-smoothing ones.

Table 1. RMS values of acceleration residuals $\Delta\ddot{x}_i$ (mm), $\Delta t = 5$ s

	$\sigma_{x_i} = 1$ cm			$\sigma_{x_i} = 2$ cm		
	$\Delta\ddot{x}_1$	$\Delta\ddot{x}_2$	$\Delta\ddot{x}_3$	$\Delta\ddot{x}_1$	$\Delta\ddot{x}_2$	$\Delta\ddot{x}_3$
GN	1.45	1.46	1.46	2.91	2.92	2.91
PR	0.16	0.16	0.16	0.32	0.32	0.32

The difference in RMS values between them are almost one order of magnitude. But this is not the whole truth. Figures 1 and 2 illustrate the amplitude spectra of the residuals in column 4 of Table 1. The spectra are identic in the

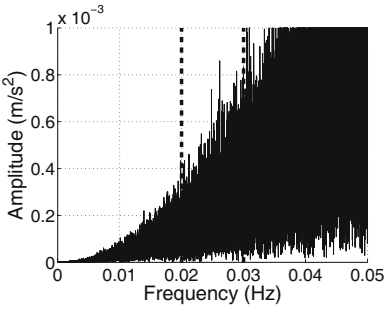

Fig. 1. Amplitude spectrum of acceleration residuals applying GN

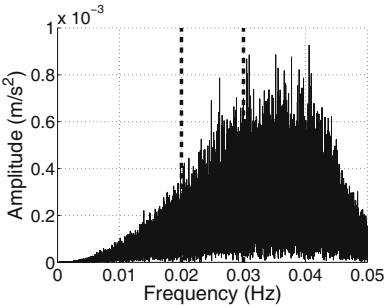

Fig. 2. Amplitude spectrum of acceleration residuals applying PR

long-wavelength part, namely up to approx. 30 mHz. The smoothing behavior dominates primarily at higher frequencies causing the differences of the RMS values in the time domain. In terms of terrestrial gravity field recovery 30 mHz corresponds to a resolution up to $L \approx 90$. This is in the range of what can be expected at most by kinematic orbit analysis, respectively what is reasonable to recover based on hl-SST observations since gradiometry covers the medium- to short-wavelength part of the gravitational spectrum. Thus, the method for numerical differentiation applying the acceleration approach is not restricted.

2.3 GOCE hl-SST Gravity Field Solutions

Numerical studies are based on a simulated GOCE data set covering one month of observation data with a sampling rate of $\Delta t = 5\,\mathrm{s}$, provided by the IAG Section II Special Commission VII (SC7). The EGM96 up to degree and order $L = 300$ is used to calculate synthetic orbit information as well as GGs with respect to the local orbit reference frame (LORF). Kinematic orbit analysis is applied to recover the terrestrial gravitational field up to degree and order $L = 100$ without any regularization. The results in terms of empirical degree error RMS are presented in Figs. 3 and 4. Due to the polar gap problem the orders $m < 5$ are not considered. Assuming non-correlated noise of 2 cm for each position coordinate a resolution up to degree $l = 70$ can be achieved whereas even $l = 80 - 85$ is reached for the more optimistic noise level of $\sigma_{x_i} = 1\,\mathrm{cm}$. Concerning the numerical differentiation method, the estimates vary for the low degrees up to approx. $l = 30$. Table 2 proves the statement that the method for numerical differentiation doesn't influence the gravity field recovery procedure significantly. The latitude weighted geoid

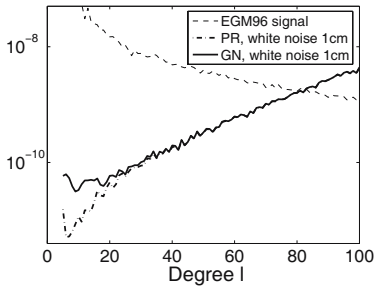

Fig. 3. Degree error RMS of hl-SST analysis with position error $\sigma_{x_i} = 1\,\mathrm{cm}$

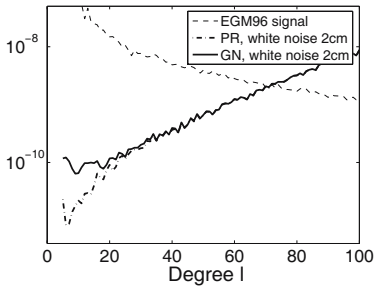

Fig. 4. Degree error RMS of hl-SST analysis with position error $\sigma_{x_i} = 2\,\mathrm{cm}$

errors (weighted with $\cos\varphi$) between the estimate and the a priori parameter set for data simulation yield almost the same results for both GN and PR.

Table 2. Latitude weighted RMS values of geoid errors (mm)

resolution L	maximal latitude $\pm 83^\circ$				maximal latitude $\pm 90^\circ$			
	$\sigma_{x_i} = 1\,\mathrm{cm}$		$\sigma_{x_i} = 2\,\mathrm{cm}$		$\sigma_{x_i} = 1\,\mathrm{cm}$		$\sigma_{x_i} = 2\,\mathrm{cm}$	
	GN	PR	GN	PR	GN	PR	GN	PR
70	0.89	0.88	1.78	1.77	0.85	0.85	1.70	1.69
80	1.61	1.60	–	–	1.55	1.54	–	–

3 SGG Analysis Based on Tensor Invariants

Differential mode measurements of the GOCE gradiometer lead to the gravitational tensor $\mathsf{U}_\mathrm{E} = (\mathbf{e}_i \otimes \mathbf{e}_j)\mathbf{U}_\mathrm{E}\,;\, i,j = 1,2,3$. The GGs $U_{ij} = U_{ji}$ are linear functionals of the Earth gravity field, namely the second derivatives of the terrestrial gravitational potential, compare (4). Assembling the accelerometers according to the diamant configuration (ESA, 1999), the main diagonal elements as well as the component U_{13} can be determined with an accuracy of about $6\,\mathrm{mE\,Hz^{-1/2}}$. The remaining GGs are provided three orders of magnitude worse.

$$(\mathbf{e}_i \otimes \mathbf{e}_j)\mathbf{U}_\mathrm{E} = \mathrm{grad} \otimes \mathrm{grad}\, U_\mathrm{E}(\lambda, \varphi, r) \tag{4}$$

Different methods use the observation model (4) for gravity field recovery. Dependent on the kind of data processing they are split in two groups, the space-wise and time-wise approach. For the first one, the analysis procedure is formulated in terms of a fixed boundary value problem (BVP). The time-wise approach treats the measurements in space as a time series. Solving the full normal equation system by brute-force inversion leads directly to an estimate

for the unknown parameter vector. Compared to that the parameterization of (4) with inclination functions (Kaula, 1966) leads to the representation of the functional model in lumped coefficients, denoted as the time-wise approach in the frequency-domain. This method requires simplified assumptions to the orbit geometry combined with an iterative analysis process, referred to as the semi-analytical approach. The different techniques are described in Rummel et al. (1993). Further details can be found in e.g. Colombo (1981), Schuh (1996), Klees et al. (2000), Sneeuw (2000) and Pail and Plank (2002).

The accuracy of the GGs is dependent on the underlying frame of reference. This is due to the influence of the poorly known tensor elements U_{12} and U_{23}. Tensor transformation leads the transformed quantities to be a linear combination of the original components of different accuracy levels and should therefore be avoided. Actually, due to the elimination of the field emission electric propulsion (FEEP) thrusters (Saccoccia et al., 2000) from the GOCE configuration the satellite is assumed to oscillate periodically about its yaw-axis. Altogether, the orientation of the satellite in space is a delicate topic. Gravity gradient tensor invariants are free of these demands.

3.1 Methodology

The invariant properties of the gravitational tensor $\mathsf{U}_\mathrm{E} = (\mathbf{e}_i \otimes \mathbf{e}_j)\mathbf{U}_\mathrm{E}$ come along with the solution of the eigenvalue problem (5) of the coefficient matrix $\mathbf{U}_\mathrm{E}$. The cubic characteristic equation (6) is composed of the eigenvalues λ_i, $i = 1, 2, 3$ and the polynomial coefficients I_1, I_2 and I_3. They are invariant with respect to the underlying reference frame, respectively reference frame rotations, and therefore denoted as tensor invariants. For the symmetric gravitational tensor they look like shown in (7) to (9).

$$\det(U_{ij} - \lambda\delta_{ij}) = 0 \tag{5}$$

$$\lambda^3 - I_1\lambda^2 + I_2\lambda - I_3 = 0 \tag{6}$$

$$I_1 = \operatorname{tr}\mathbf{U}_\mathrm{E} \tag{7}$$

$$I_2 = \frac{1}{2}\left[\operatorname{tr}\mathbf{U}_\mathrm{E}^2 - (\operatorname{tr}\mathbf{U}_\mathrm{E})^2\right] \tag{8}$$

$$I_3 = \det\,\mathbf{U}_\mathrm{E} \tag{9}$$

Inserting the harmonic series expansion of the GGs in the formulae above finally leads to the functional model for invariant analysis as presented in (10) to (12).

$$I_1 = \frac{GM}{R^3} \sum_{i=0}^{\infty} \sum_{j=0}^{i} \left(\frac{R}{r}\right)^{i+3} S_{ij}^1(\varphi) \left[c_{ij} \cos(j\lambda) + s_{ij} \sin(j\lambda)\right] \tag{10}$$

$$\begin{aligned} I_2 = \left(\frac{GM}{R^3}\right)^2 \sum_{i=0}^{\infty} \sum_{j=0}^{i} \sum_{k=0}^{\infty} \sum_{l=0}^{k} \left(\frac{R}{r}\right)^{i+k+6} \{ \\ K_{ijkl}^1(\varphi) \left[-c_{ij} \sin(j\lambda) + s_{ij} \cos(j\lambda)\right] \left[-c_{kl} \sin(l\lambda) + s_{kl} \cos(l\lambda)\right] + \\ K_{ijkl}^2(\varphi) \left[c_{ij} \cos(j\lambda) + s_{ij} \sin(j\lambda)\right] \left[c_{kl} \cos(l\lambda) + s_{kl} \sin(l\lambda)\right] \} \end{aligned} \tag{11}$$

$$\begin{aligned} I_3 = \left(\frac{GM}{R^3}\right)^3 \sum_{i=0}^{\infty} \sum_{j=0}^{i} \sum_{k=0}^{\infty} \sum_{l=0}^{k} \sum_{m=0}^{\infty} \sum_{n=0}^{m} \left(\frac{R}{r}\right)^{i+k+m+9} \{ \\ D_{ijklmn}^1(\varphi) \left[c_{ij} \cos(j\lambda) + s_{ij} \sin(j\lambda)\right] \\ \times \left[-c_{kl} \sin(l\lambda) + s_{kl} \cos(l\lambda)\right] \left[-c_{mn} \sin(n\lambda) + s_{mn} \cos(n\lambda)\right] + \\ D_{ijklmn}^2(\varphi) \left[c_{ij} \cos(j\lambda) + s_{ij} \sin(j\lambda)\right] \\ \times \left[c_{kl} \cos(l\lambda) + s_{kl} \sin(l\lambda)\right] \left[c_{mn} \cos(n\lambda) + s_{mn} \sin(n\lambda)\right] \} \end{aligned} \tag{12}$$

The coefficient functions $S_{ij}^1(\varphi), K_{ijkl}^{1,2}(\varphi)$ and $D_{ijklmn}^{1,2}(\varphi)$ contain the Legendre functions as well as their first and second derivatives. Analysis of the first invariant leads to the trivial solution $\mathbf{0}$ since $\operatorname{tr} \mathbf{U}_{\mathrm{E}} \equiv 0$ holds for the gravitational tensor. Thus, I_1 can't be used for potential field recovery. Non-linearity of the functional models for I_2 and I_3 makes invariant analysis to become an iterative process. Linearization of (11) and (12) with respect to the unknown coefficients c_{pq}, respectively s_{pq}, is performed by summation of the partial derivatives for each combination of $p = \text{const}$ and $q = \text{const}$, as outlined in (13) and (14).

$$\frac{\partial I_2}{\partial c, s_{p,q=\text{const}}} = \frac{\partial I_2}{\partial c, s_{i=p,j=q}} + \frac{\partial I_2}{\partial c, s_{k=p,l=q}} \tag{13}$$

$$\frac{\partial I_3}{\partial c, s_{p,q=\text{const}}} = \frac{\partial I_3}{\partial c, s_{i=p,j=q}} + \frac{\partial I_3}{\partial c, s_{k=p,l=q}} + \frac{\partial I_3}{\partial c, s_{m=p,n=q}} \tag{14}$$

For the first iteration an approximate solution for linearization has to be introduced. Within this contribution the OSU86F model is used. Note that data simulation is based on the EGM96. Actually, the iterative procedure converges very fast. For studies using noise-free simulated data, the final solution is reached after the second or even first iteration, i.e. the linearization error is small.

3.2 Series Truncation

Unfortunately the coefficient functions $K_{ijkl}^2(\varphi)$ and $D_{ijklmn}^{1,2}(\varphi)$ are not symmetric with respect to index permutation, i.e. $K_{pqkl}^2(\varphi) \neq K_{ijpq}^2(\varphi)$ etc. holds.

Thus, for the setup of the linearized models (13) and (14) four fold, respectively six fold, nested sums have to be evaluated. Combined with an iterative procedure, especially for a high-resolution gravity field estimate, the strict method is not applicable from the computational point of view. However, the full computation can be avoided by early truncation of the inner loops (15), which virtually leads to the same results.

$$i_{\max} = L, \;\; k_{\max}, m_{\max} \ll L \tag{15}$$

For noise-free SC7 data, Fig. 5 presents degree error RMS differences between SGG analysis based on the radial component U_{33} and solutions after the first iteration performing analysis of the second invariant with series truncation for the inner loops at degree 3, respectively degree 0. Due to the polar gap problem the plots don't contain low orders up to $m = 6$. Apart from the low degrees, the sum of both linearization error and truncation error is below the empirical error curve of the non-iterative estimate. Thus, early series truncation is an adequate tool to decrease runtime for invariant analysis dramatically.

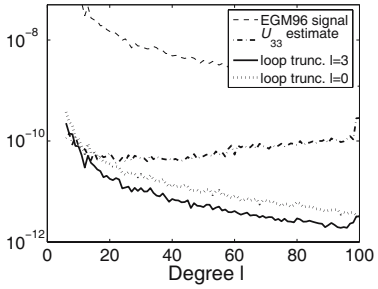

Fig. 5. Degree error RMS between U_{33} analysis estimate and I_2 solutions dependent on series truncation

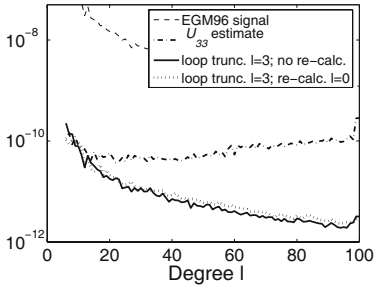

Fig. 6. Degree error RMS between U_{33} analysis estimate and I_2 solutions dependent on re-calculation of GGs

3.3 Re-calculation of Tensor Elements

Besides the computational effort for invariant analysis a further aspect has to be considered, namely the amalgamation of GGs, compare (8) and (9). The second and the third invariant are composed of products between both the tensor elements of high and reduced accuracy. Thus, the overall accuracy of invariants would be decreased as well. This problem can be circumvented by re-calculation of the elements U_{12} and U_{23} from iteration to iteration. The course of action is outlined in Fig. 7. Starting from the linearized observation equation, for the first iteration an a priori gravity field parameter set is used to calculate synthetic values for the "unknown" tensor elements U_{12} and U_{23},

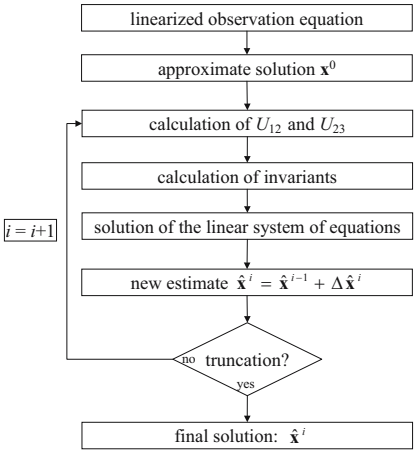

Fig. 7. Re-calculation of GGs

respectively the pseudo-observations of type invariants. For successive iterations the actual estimate is used to update the tensor component calculation. In Fig. 6 additionally to series truncation of the inner loops at degree 3, the simulated GGs U_{12} and U_{23} have been replaced by synthetic values based on the OSU86F model only considering degree 0 for evaluation. The replaced tensor elements don't influence the result significantly even when truncating their calculation at $L = 0$. That means, the analysis procedure is insensitive to the deviation of the real values from the synthetic ones. Thus, re-calculation of GGs is an adequate tool to overcome the difficulties of allocating the pseudo-observations for invariant analysis.

4 High Performance Computing in Gravity Field Research

From the computational point of view the problem dimension for GOCE data analysis has to be treated according to both memory requirement and runtime. Parallelization of the least squares adjustment procedure using multiprocessor architectures is indispensable for solving for the unknown gravity field parameters. During the operational mode of the GOCE mission observations amount to several millions of gradiometer measurements as well as position coordinates of the spacecraft. Whereas the setup of the design matrix, respectively the normal matrix, can be done blockwise, for direct inversion of the normal equation system (NES), referred to as the brute-force approach, at least one triangle of the symmetric normal matrix has to be kept in the memory. For a resolution of the terrestrial gravity field up to degree and order $L = 300$ this equals a memory availability of 33 GB. Ordinary PCs don't

come along with these requirements. Remedy can be found by using iterative solvers such as conjugate gradient (CG) methods (Hestenes and Stiefel, 1952) or the LSQR algorithm (Paige and Saunders, 1982a,b) which have been applied successfully for potential field recovery (Ditmar and Klees, 2002; Baur and Austen, 2005). Due to their design, matrix-matrix operations are replaced by repeated vector-vector operations. Thus, memory requirements are small. Despite of that, for both the brute-force approach and iterative solvers runtime of the analysis process makes parallelization of the implementation necessary.

4.1 Parallelization

With regard to the brute-force approach the setup of the design matrix $\mathbf{A}$ and computation of the normal matrix $\mathbf{N}$ is done blockwise according to (18).

$$\mathbf{A}\mathbf{x} = \mathbf{y} \tag{16}$$

$$\mathbf{A}^T\mathbf{A}\hat{\mathbf{x}} = \mathbf{A}^T\mathbf{y} \leftrightarrow \mathbf{N}\hat{\mathbf{x}} = \mathbf{b} \tag{17}$$

$$\mathbf{N} = \mathbf{A}_1^T\mathbf{A}_1 + ... + \mathbf{A}_j^T\mathbf{A}_j = \sum_{i=1}^{j} \mathbf{A}_i^T\mathbf{A}_i = \sum_{i=1}^{j} \mathbf{N}_i \tag{18}$$

This approach is indispensable, given that for a large amount of observations and many unknowns the design matrix can not be kept in the main memory. Indeed, a blockwise procedure even allows for the use of parallel matrix-matrix and matrix-vector routines provided by the numerical libraries such as e.g. Lapack and Blas (Anderson et al., 1999) to repeatedly compute $\mathbf{N}_i = \mathbf{A}_i^T\mathbf{A}_i$. Further parallelization is achieved for the setup of each design matrix block $\mathbf{A}_i$ by distributing the observations contributing to each block to several central processing units (CPUs).

Due to the character of iterative methods, matrix-matrix and matrix-vector multiplications are avoided by means of repeated vector-vector operations. Since neither the design matrix nor the normal matrix must be kept in the main memory, storage requirements are by far smaller as compared to direct solvers at the expense of an increased amount of operations. Fortunately, these multiplications can be done separately for each observation. Additionally, the major computational costs occur within the calculation of the design matrix. It is therefore reasonable to distribute the amount of observations on several CPUs of a multiprocessor computation platform to build up the design matrix line by line, each line referring to a separate observation. Within the scope of this contribution it is exclusively concentrated on the brute-force approach.

4.2 High Performance Computing

Different platform architectures for parallel implementation with OpenMP and MPI have been considered to investigate their benefit for the setup and

solution of the NES by means of the brute-force approach. All the systems are supported by the High Performance Computing Center Stuttgart (HLRS), namely (i) NEC TX-7 (ii) NEC SX-6 (iii) Cray Strider. The architecture of platform (i) is ccNUMA, i.e. similar to shared-memory systems. Platform (ii) is, considering only one node, a shared-memory array processor system. Platform (iii) is in principle (disregarding that each single node is in fact a SMP node of 2 CPUs) a distributed-memory cluster. Table 3 lists some specific values of the super computers. To evaluate the performance of the least squares procedure regarding the different platforms a comparable test peak performance according to the last column of Table 3 has been chosen. Table 4 summarizes the performance, efficiency respectively, of a test scenario with maximal resolution $L = 50$ and half a million of observations of type hl-SST. The SX-6 is more than three minutes slower than the TX-7 and only achieves

Table 3. Specific values of computation platforms (PP–peak performance)

platform	architecture	number of CPUs	main memory (GB)	theoretical PP (GFlops)	test PP (GFlops)
NEC TX-7	ccNUMA	16	240	$16 \cdot 6$	$8 \cdot 6 = 48$
NEC SX-6	cluster	$6 \cdot 8$	$6 \cdot 64$	$6 \cdot 8 \cdot 9$	$5 \cdot 9 = 45$
Cray Strider	cluster	$125 \cdot 2$	$125 \cdot 4$	$125 \cdot 2 \cdot 4$	$12 \cdot 4 = 48$

Table 4. Achieved performance for hl-SST analysis

platform	wall time	user time	performance (GFlops)	efficiency (%)
NEC TX-7	6 m 58 s	54 m 7 s	25.4	53
NEC SX-6	10 m 22 s	38 m 32 s	16.6	37
Cray Strider	9 m 16 s	111 m 12 s	18.6	39

an efficiency of 37% as compared to 53% for the ccNUMA architecture. This is surprising since vectorization of the algorithm should increase the performance significantly. Actually, the efficiency of the platform is decreased by comparatively time-consuming data reading. The time for real computations is about seven minutes which corresponds to a performance of 24.6 GFlops, respectively an efficiency of 55%. This is still disappointing but due to the moderate problem dimension. To proof that, an additional calculation has been performed on the SX-6 with a resolution up to $L = 100$ for the terrestrial gravitational potential. The impact of vectorization is obvious since the efficiency amounts to 88% which is near to the theoretical peak performance. Thus, the array processor system SX-6 is suited very well for the brute-force approach. The result for the Opteron cluster Cray Strider turns out to be

worse. This has been expected in advance since compared to the TX-7 the cache of the Opteron CPUs is considerably smaller. Additionally, runtime costs for the communication between the cluster nodes by using MPI has to be accepted.

The impact of HPC for GOCE gravity field recovery is summarized in Tables 5 and 6. The calculations are performed on the TX-7 dependent on the number of observations and the number of threads used. The runtimes in

Table 5. Impact of HPC for hl-SST analysis ($L = 100$)

number of observations (mill.)	number of CPUs	time setup $\mathbf{A}$ (min)	time setup $\mathbf{N}, \mathbf{b}$ (min)	time NES inversion (min)
1.5	1	8	560	4
1.5	4	4	140	1
1.5	8	2	70	0.5

Table 6 correspond to SGG analysis on the level of gravity gradients, respectively second invariant analysis with truncation of the inner loops at degree 0. Decorrelation is not applied regarding the time to set up the design matrix $\mathbf{A}$. For both hl-SST and SGG analysis optimal scaling is achieved with respect to the number of observations as well as the number of CPUs. The main computational effort is within the calculation of the NES, namely the algebraic operations $\mathbf{N} = \mathbf{A}^T\mathbf{A}$ and $\mathbf{b} = \mathbf{A}^T\mathbf{y}$. The time for NES inversion is comparatively short.

Table 6. Impact of HPC for SGG analysis ($L = 200$)

number of observations (mill.)	number of CPUs	time setup $\mathbf{A}$ (min)	time setup $\mathbf{N}, \mathbf{b}$ (min)	time NES inversion (min)
0.5	1	320	2700	160
0.5	4	80	680	40
0.5	8	40	340	20
1.5	8	120	1050	20

5 Conclusions

For purposes of estimating a GOCE-only gravity field we have analyzed hl-SST data using the acceleration approach. Based on one month of kinematic orbit data, dependent on the error budget at least a resolution up to degree $L = 70$ in terms of spherical harmonics in the long-wavelength part can be

achieved. The method for numerical differentiation of the spacecraft's position information is not restricted.

Invariant analysis has been proven to be applicable in three-dimensional gradiometry. It is associated, though, with a more complicated processing strategy as compared to conventional approaches, in which the main diagonal tensor elements are analyzed directly. Both the enormous numerical effort and the mixture of high and low accuracy tensor components can be circumvented by early series truncation, respectively re-calculation of the poorly known gravitational gradients from iteration to iteration based on the previous estimate of the unknown parameter vector. Stochastic properties of the invariant approach have not been treated yet.

Parallel implementation of the least squares adjustment procedure on different HPC platforms has been achieved successfully. Linear scaling in runtime with respect to both the number of observations and the number of CPUs together with the use of optimized numerical libraries ensure highly efficient data processing.

Acknowledgement. This is publication No. 155 of the program GEOTECHNOLOGIEN of BMBF and DFG, Grant 03F0329B. The authors thank the High Performance Computing Center Stuttgart (HLRS) for the opportunity to use their computing facilities.

References

Anderson E, Bai Z, Bischof C, Blackford S, Demmel J, Dongarra J, Du Croz J, Greenbaum A, Hammarling S, McKenney A, Sorensen D (1999) LAPACK Users' Guide (third edition). SIAM Publications, Philadelphia

Baur O, Austen G (2005) A parallel iterative algorithm for large-scale problems of type potential field recovery from satellite data. Manuscript submitted to Advances in Geosciences

Colombo O (1981) Numerical methods for harmonic analysis on the sphere. Department of Geodetic Science, Report No. 310, Ohio State University, Columbus, Ohio

Ditmar P, Klees R (2002) A method to compute the Earth's gravity field from SGG/SST data to be acquired by the GOCE satellite. Delft University Press

ESA (1999) Gravity Field and steady-state ocean circulation - The four candidate Earth explorer core missions. ESA Publications Division, ESA SP-1233(1), ESTEC, Noordwijk, The Netherlands

ESA (2000) From Eötvös to milligal. Final report ESA/ESTEC, Contract No. 13392/NL/GD

Földváry L, Švehla D, Gerlach C, Wermuth M, Gruber T, Rummel R, Rothacher M, Frommknecht B, Peters T, Steigenberger P (2005) Gravity Model TUM-2Sp Based on the Energy Balance Approach and Kinematic CHAMP Orbits. In: Reigber C, Lühr H, Schwintzer P, Wickert J (eds.) Earth Observation with CHAMP - Results from Three Years in Orbit, 13–16, Springer, Berlin

Hestenes MR, Stiefel E (1952) Methods of conjugate gradients for solving linear systems. Journal of Research of the National Bureau of Standards, 49, 409–436

Kaula WM (1966) Theory of satellite geodesy. Blaisdell, Waltham, MA

Klees R, Koop R, Visser P, van den IJssel J (2000) Efficient gravity field recovery from GOCE gravity gradient observations. JoG, 74, 561–571

Maeß G (1988) Vorlesungen über numerische Mathematik II. Akademie Verlag, Berlin

Mayer-Gürr T, Ilk KH, Eicker A, Feuchtinger M (2005) ITG-CHAMP01: A CHAMP Gravity Field Model from Short Kinematic Arcs over a One-Year Observation Period. JoG, 78, 462–480

Paige CC, Saunders MA (1982a) LSQR: An algorithm for sparse linear equations and sparse least squares. ACM Transactions on Mathematical Software, 8, 43–71

Paige CC, Saunders MA (1982b) LSQR: Sparse linear equations and least squares problems. ACM Transactions on Mathematical Software, 8, 195–209

Pail R, Plank G (2002) Assessment of three numerical solution strategies for gravity field recovery from GOCE satellite gravity gradiometry implemented on a parallel platform. JoG, 76, 462–474

Reigber C, Jochmann H, Wnsch J, Petrovic S, Schwintzer P, Barthelmes F, Neumayer KH, König R, Förste C, Balmino G, Biancale R, Lemoine JM, Loyer S, Perosanz F (2005) Earth Gravity Field and Seasonal Variability from CHAMP. In: Reigber C, Lühr H, Schwintzer P, Wickert J (eds.) Earth Observation with CHAMP - Results from Three Years in Orbit, 25–30, Springer, Berlin

Reubelt T, Austen G, Grafarend EW (2003) Harmonic analysis of the Earth's gravitational field by means of semi-continuous ephemerides of a low Earth orbiting GPS-tracked satellite. Case study: CHAMP. JoG, 77, 257–278

Reubelt T, Götzelmann M, Grafarend EW (2005) A new CHAMP gravitational field model based on the GIS acceleration approach and two years of kinematic CHAMP data. Manuscript submitted to Advances in Geosciences

Rummel R (1986) Satellite Gradiometry. In: Sünkel H (ed.) Mathematical and Numerical Techniques in Physical Geodesy, Lecture Notes in Earth Sciences 7, Springer

Rummel R, Sansò F, van Gelderen M, Brovelli M, Koop R, Miggliaccio F, Schrama E, Scerdote F (1993) Spherical harmonic analysis of satellite gradiometry. Netherlands Geodetic Commission, New Series, 39

Saccoccia G, Gonzales del Amo J, Estublier D (2000) Electric Propulsion: A Key Technology for Space Missions in the New Millenium. ESA Bulletin 101, ESTEC, Noordwijk, The Netherlands

Schuh WD (1996) Tailored Numerical Solution Strategies for the Global Determination of the Earth's Gravity Field. Mitteilungen der Geodätischen Institute der TU Graz, 81, Graz

Sneeuw N (2000) A semi-analytical approach to gravity field analysis from satellite observations. DGK, Series C, No. 527, Munich